Desalination and Water Treatment
www.deswater.com
doi: 10.5004/dwt.2021.27360

228 (2021) 351–361
July

Synthesis of novel $Bi_2O_3/BiVO_4/Ag_3VO_4$ heterojunction photocatalyst with enhanced photocatalytic activity under visible light irradiation

Chung-Hsin Wu[a,*], Cheng-Di Dong[b], Chiu-Wen Chen[b], Yi-Li Lin[c], Yu-Rong Cheng[d], Guo-Yi Lee[a]

[a]*Department of Chemical and Materials Engineering, National Kaohsiung University of Science and Technology, 415 Chien Kung Road, Kaohsiung, Taiwan, Tel. +886-7-3814526; Fax: 886-7-3830674; email: wuch@nkust.edu.tw (C.-H. Wu), Tel. +886-7-3814526; email: jwge74540918@gmail.com (G.-Y. Lee)*
[b]*Department of Marine Environmental Engineering, National Kaohsiung University of Science and Technology, Kaohsiung, Taiwan, Tel. +886-7-3617141; email: cddong@nkust.edu.tw (C.-D. Dong), Tel. +886-7-3617141; email: cwchen@nkust.edu.tw (C.-W. Chen)*
[c]*Department of Safety, Health and Environmental Engineering, National Kaohsiung University of Science and Technology, Kaohsiung, Taiwan, Tel. +886-7-6011000; email: yililin@nkust.edu.tw*
[d]*Department of Fisheries Production and Management, National Kaohsiung University of Science and Technology, Kaohsiung, Taiwan, Tel. +886-7-3617141; email: yrcheng@nkust.edu.tw*

Received 15 February 2021; Accepted 25 April 2021

ABSTRACT

In this investigation, Bi_2O_3 (BOS), $BiVO_4$ (BVO) and Ag_3VO_4 (AVO) are used to generate a novel $Bi_2O_3/BiVO_4/Ag_3VO_4$ (BBA) heterojunction photocatalyst via a two-step hydrothermal/solvothermal procedure. BVO/AVO composites were synthesized by a single-step hydrothermal process with different BVO/AVO molar ratios. C.I. Reactive Red 2 (RR2) was used as the parent compound to evaluate the photocatalytic activity of the synthesized photocatalysts under ultraviolet (UV) and visible light (Vis.) irradiation. The morphological, structural, and spectroscopic properties of the synthesized photocatalysts were obtained by scanning electron microscopy, transmission electron microscopy (TEM), X-ray diffraction (XRD), UV-Vis. diffuse reflectance spectral analysis, specific surface area analysis, photoluminescence spectral analysis and X-ray photoelectron spectroscopy (XPS). The XRD, TEM and XPS results revealed the coexistence of AVO, BVO and BOS photocatalysts in the BBA hybrid material. The optimal BVO/AVO molar ratio for forming BVO/AVO composite was unity and the photocatalyst that was formed at this ratio was denoted as BA(1). The rate is constant of BBA in the Vis. photocatalysis of the degradation of RR2 was approximately 1.4, 8.9, 12.3 and 1.5 times those of BOS, BVO, AVO and BA(1), respectively. This study suggests that photo-generated holes were mostly responsible for the photocatalytic activity of BBA. The enhanced photocatalytic performance of BBA was attributed to the reduced probability of recombination of the photo-generated electrons and holes.

Keywords: $BiVO_4$; Ag_3VO_4; Bi_2O_3; Heterojunction; Photocatalyst; Photodegradation

1. Introduction

Semiconductor photocatalysis is a cost-effective and environmentally friendly method for solar energy utilization and environmental remediation. New photocatalysts that are effective under visible light (Vis.) must be developed because the sun emits such light at high intensity. The ideal photocatalyst has a low bandgap, has high dispersibility, is non-toxic, resists photo-corrosion, and exhibits outstanding photocatalytic activity in the degradation of pollutants under Vis. illumination.

* Corresponding author.

Ag_3VO_4 (AVO) is an n-type semiconductor that was first synthesized by Konta et al. [1]. It exhibits photocatalytic activity in the evolution of O_2 from H_2O under Vis. irradiation and has therefore attracted considerable attention. However, AVO suffers from serious photo-corrosion and the recombination of photo-generated holes (h^+) and electrons during photocatalysis. $BiVO_4$ (BVO) is also an n-type semiconductor, which has high chemical stability and photo-stability. The photocatalytic behavior of pure BVO must be improved because of the rapid recombination of photo-induced carriers therein [2–4].

To solve the problems that are associated with BVO and AVO, the combination of BVO and AVO with another photocatalyst to form a heterojunction has been proposed. Heterojunction structures have better photocatalytic properties, such as light utilization efficiency, charge separation, and carrier lifetime, than single-component photocatalysts owing to the synergistic properties of their constituents [5,6]. The heterojunction structure improves the transfer of the photo-generated electrons and h^+, exhibits strong redox ability and increases the activity of the photocatalysts.

The 40% BVO/AVO (BA) composite exhibits excellent photocatalytic methylene blue degradation properties with a rate constant of 0.05588 min^{-1}, which is 22.76 and 1.76 times higher than those of BVO (0.00247 min^{-1}) and AVO (0.03167 min^{-1}), respectively [5]. Yan et al. [7] synthesized a sample with a 10:1 mole ratio of BVO:AVO and found that it had the highest photocatalytic activity among all of those that they prepared with various mole ratios. Rhodamine B was completely degraded (95.9%) by BVO and AVO at this ratio under Vis. irradiation in 20 min, which was 1/10 and 1/3.4 times as long as required with pristine BVO and AVO, respectively. Wang and Cao [8] synthesized a novel BA heterojunction photocatalyst and found that the 4% AVO/BVO heterojunction provided the highest rate constant, which was around 17.2 and 3.1 times higher than those of pure BVO and AVO, respectively. Wang and Cao [8] showed that this enhancement was due mainly to the formation of a suitable heterojunction structure with close interfacial contact between BVO and AVO, causing the effective separation of photo-generated electron-hole pairs. Zhao et al. [9] found that 24% $AgVO_3$/BVO exhibits the highest photocatalytic performance, outperforming pure BVO and $AgVO_3$ in particular. This enhanced photocatalytic performance is attributed to the fact that the built-in electric field promotes the transfer of photo-generated charges between the $AgVO_3$ and BVO, and to an increase in the lifetime of the charge carriers [5,7,9].

Combining p-type and n-type semiconductors is the most effective way to improve photocatalytic activity because doing so forms a p-n heterojunction. A p-n heterojunction, which has an internal electric field, can considerably promote the separation of photo-generated charge carriers and improve photodegradation efficiency [10–13]. Recently, the p-type Bi_2O_3 (BOS) semiconductor, as the simplest bismuth oxide, has attracted considerable interest owing to its several favorable properties, such as a wide bandgap (2.0–3.96 eV), good electrochemical performance, and high oxygen-ion conductivity [14]. Although BOS/BVO [3,11,13–15] and BOS/AVO [15,16] have already been developed, the development of novel Vis.-induced photocatalysts is being pursued. Accordingly, in this study, BOS is combined with BA to form a p-n heterojunction to improve the photoactivity of BVO, AVO or BA. To the best of our knowledge, the hybridization of BA with BOS for photocatalysis has not been achieved. This method may form a highly efficient heterojunction that can degrade organic pollutants. In this study, the two-step hydrothermal/solvothermal procedure was used to synthesize the BOS/BVO/AVO (BBA) heterojunction photocatalyst, whose photocatalytic activity in the degradation of C.I. Reactive Red 2 (RR2) under ultraviolet (UV) irradiation was compared with that under Vis. irradiation. The objectives of this study are (i) to synthesize BA with various BVO/AVO molar ratios; (ii) to couple BOS with BA at the optimal BVO/AVO molar ratio to generate the novel BBA; (iii) to measure the surface characteristics and compare the photocatalytic activities of the synthesized photocatalysts; (iv) to identify the active reaction species in BBA; and (v) to propose possible mechanisms by which the photoactivity of BBA is enhanced.

2. Materials and methods

2.1. Materials

Bismuth(III) nitrate ($Bi(NO_3)_3{\cdot}5H_2O$), trisodium citrate (TCD, $Na_3C_6H_5O_7{\cdot}2H_2O$), ammonium metavanadate (NH_4VO_3), ethylene glycol (EG), sodium hydroxide (NaOH), nitric acid (HNO_3), sodium nitrite ($NaNO_2$), potassium chromate (K_2CrO_4) and disodium ethylenediaminetetraacetate (EDTA-2Na, $C_{10}H_{14}N_2O_8Na_2{\cdot}2H_2O$) were all purchased from Katayama (Japan). EG was used as a solvent in the solvothermal process. Silver nitrate ($AgNO_3$) and RR2 ($C_{19}H_{10}Cl_2N_6Na_2O_7S_2$) were obtained from Sigma-Aldrich (USA). Sodium orthovanadate (Na_3VO_4) and isopropanol (IPA) were obtained from Alfa Aesar (USA) and J.T. Baker (USA), respectively. All chemicals were of analytical reagent grade and used without further purification or treatment. Deionized water (D.I. water) was used throughout the study.

2.2. Procedures for synthesizing photocatalysts

The BVO, AVO and BA photocatalysts were prepared using single-step hydrothermal processes; the BOS was formed by a single-step solvothermal process. The procedures for synthesizing BOS, BVO and AVO were modified from those of Wu et al. [15]. The BBA heterojunction was synthesized by a two-step hydrothermal/solvothermal process.

2.2.1. Synthesis of BOS

A 4.949 g mass of $Bi(NO_3)_3{\cdot}5H_2O$ was added to 140 mL EG to form solution A. The pH of this solution was adjusted to pH 7 by adding 10 M NaOH or HNO_3 and stirring (600 rpm) for 30 min. The adjusted solution was sealed in a 200 mL Teflon-lined stainless steel autoclave and heated at 393 K under self-generated pressure for 6 h; it was then left to cool naturally to room temperature.

The precipitates thus obtained were collected by filtration and washed using 50 mL 95% ethanol and 100 mL D.I. water to remove any residual impurities. The samples were finally dried in air at 333 K for 24 h to yield BOS.

2.2.2. Synthesis of BVO

A 2.4745 g mass of $Bi(NO_3)_3{\cdot}5H_2O$ was added to 60 mL 2 M HNO_3 to form solution B. A 0.5850 g mass of NH_4VO_3 was dissolved in 60 mL 2 M NaOH to yield solution C. A 0.4456 g mass of TCD was dissolved in 20 mL D.I. water to form solution D. Solutions B, C and D were mixed and adjusted to pH 7 by adding 10 M NaOH or HNO_3 and stirring (600 rpm) for 30 min. The adjusted mixture was sealed in a 200 mL Teflon-lined stainless steel autoclave and heated at 473 K under self-generated pressure for 12 h. The subsequent steps and conditions for the formation of BVO were as for that of BOS.

2.2.3. Synthesis of AVO

A 2.5845 g mass of $AgNO_3$ and 0.9205 g of Na_3VO_4 were dissolved in 60 mL D.I. water to yield solutions E and F, respectively. Solutions D, E and F were mixed and adjusted to pH 7 by adding 10 M NaOH or HNO_3 and stirring (600 rpm) for 30 min. The adjusted mixture was sealed in a 200 mL Teflon-lined stainless autoclave and maintained at 393 K for 6 h. The subsequent steps and conditions for the formation of AVO were as for BOS.

2.2.4. Synthesis of BA and BBA heterojunctions

Three BVO/AVO molar ratios (0.5, 1.0 and 2.0) were used in the syntheses, yielding BA(0.5), BA(1) and BA(2), respectively. The details of BA(1) synthesis were as follows. Mix solutions B, C and D in beaker I and mix solutions D, E and F in beaker II. The solutions in each of the beakers were mixed and adjusted to pH 7 by stirring with the addition of 10 M NaOH or HNO_3 (600 rpm) for 30 min. A 140 mL volume of each mixture was collected; sealed in a 200 mL Teflon-lined stainless steel autoclave, and heated at 393 K under self-generated pressure for 6 h. The subsequent steps and conditions for the formation of BA(1) were as for that of BOS. To synthesize BBA, 3.8123 g synthesized BA(1) particles were added to solution A to yield a BOS/BVO/AVO molar ratio of 1/1/1. The subsequent procedure and conditions that were used to generate BBA were those used to generate BOS.

2.3. Analyses of surface characteristics

The crystalline phase of each of the synthesized photocatalysts was characterized by X-ray diffraction (XRD) with Cu-Kα radiation (Bruker D8 SSS, Germany) over a 2θ range of 20°–80°. The morphologies and microstructures of the samples were observed using scanning electron microscopy (SEM, JEOL 6330 TF, Japan) and transmission electron microscopy (TEM, JEOL 3010, Japan), respectively. The specific surface areas of the synthesized powders were measured by nitrogen adsorption/desorption using the Barrett–Emmett–Teller (BET) method (Micromeritics ASAP 2020, USA). UV-Vis diffuse reflectance spectroscopy (UV-Vis DRS, JASCO V-670, Japan) was used to investigate the optical properties of the synthesized photocatalysts. The photoluminescence (PL, Hitachi F-4500, Japan) spectra were recorded using a fluorescence spectrometer and the excitation wavelength was 400 nm. X-ray photoelectron spectroscopy (XPS) measurements were made at room temperature using a PHI 5000 Versal Probe X-ray photoelectron spectrometer (USA). The binding energies were calibrated against C 1s at 284.6 eV.

2.4. Photocatalysis experiments

The photocatalyst dosage, RR2 concentration, solution pH and temperature in all of the experiments were 0.5 g/L, 20 mg/L, pH 3, and 298 K, respectively. Photocatalysis experiments were performed in a 3 L glass reactor. A 400 W Xe lamp (200 nm < wavelength < 700 nm, UniVex BT-580, Taiwan) was used to provide UV radiation with an intensity of 30.3 mW/cm^2. A quartz that was filled with 2 M $NaNO_2$ solution was placed on top of the reactor to cut the UV and to provide Vis. [17]. Adsorption experiments were conducted in darkness. To detect the active species that were responsible for the photocatalytic reactivity, trapping experiments were performed. In a process similar to that used in the photocatalysis experiment, scavengers K_2CrO_4, EDTA-2Na and IPA were introduced into the RR2 solution before the photocatalyst was added; these were scavengers of superoxide anion radicals ($^{\bullet}O_2^-$) [18], h^+ [19,20] and hydroxyl radicals ($^{\bullet}OH$) [19,20], respectively. The reaction medium was stirred continuously at 300 rpm and aerated with air to maintain a suspension. Following sampling at known intervals, solids were separated by filtration through a 0.22 μm filter (Millipore, USA). Samples were extracted from the reactor at regular intervals and the photocatalyst was removed for spectrophotometric analysis (Hitachi U-5100, Japan). The absorbance of the supernatant was determined at the 538 nm peak to determine the concentration of RR2 at various times. The photocatalytic experiments were performed in triplicate and mean values were reported.

3. Results and discussion

3.1. Determinations of surface properties of photocatalysts

The crystalline phases of photocatalysts were identified by XRD analysis. Fig. 1 presents the XRD patterns of all synthesized photocatalysts. The observed patterns reveal that the synthesized AVO, BVO and BOS all had monoclinic structures, corresponding to JCPDs Nos. 43-0542, 14-0688 and 27-0053, respectively. The strongest characteristic diffraction peaks from BOS, BVO and AVO were at 28.2°, 28.9° and 32.3°, respectively. The diffraction peaks from BVO/AVO composites were similar to those from pure BVO and AVO, suggesting that introducing BVO did not change the crystal structure of AVO. As the BVO content in BVO/AVO composites increased, so did the intensity of the diffraction peak of BVO at a 2θ angle of 28.9° (Fig. 1). Results revealed that AVO, BVO and BOS

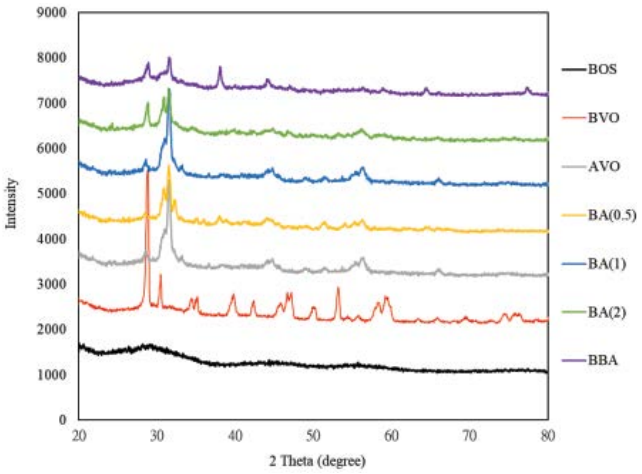

Fig. 1. XRD patterns of synthesized photocatalysts.

photocatalysts were all present in the BBA hybrid material. The principal diffraction peaks of BBA were not significantly shifted, indicating that the BOS was present as a separate phase rather than being incorporated into the BA(1) lattice.

Figs. 2 and 3 show SEM and TEM images of the synthesized photocatalysts, respectively. The BOS had a flake-like morphology with some randomly dispersed fragments (Fig. 2a). The BVO consisted of large polyhedral particles with relatively smooth surfaces (Fig. 2b). The AVO comprised mainly irregular spherical-like structures that contained some randomly dispersed nanoparticles (Fig. 2c). Fig. 2d–f show that BVO powder was immobilized on AVO particles; Fig. 2g shows that BA(1) particles were immobilized by BOS sheets. The BOS flakes had a mean width of 200 nm (Fig. 3a). BVO (Fig. 3b) and AVO (Fig. 3c) nanoparticles had average diameters of 500 and 25–40 nm, respectively. Fig. 3d shows that irregular particles (BVO) and spherical nanoparticles (AVO) mixed with each other. Fig. 3d and e reveal close interfacial contact in the BA(1) and BBA heterojunctions rather than a simple mechanical mixture of the two components. All synthesized photocatalysts exhibited significant agglomeration.

UV-Vis diffuse reflectance spectra of the synthesized photocatalysts were obtained (data not shown). All synthesized photocatalysts exhibited good optical absorption in the Vis. region. The bandgap of all photocatalysts was estimated using l (nm) = 1,240/E_g (eV), where λ and E_g are the absorption band threshold wavelength and the bandgap, respectively. The obtained bandgaps of BOS, BVO, AVO, BA(0.5), BA(1), BA(2) and BBA were 3.0, 2.4, 1.8, 1.9, 2.3, 2.3 and 2.3 eV, respectively (Table 1). The BET surface areas of the BVO/AVO composites exceeded those of pristine BVO (0.08 m^2/g) and AVO (2.18 m^2/g). The BET surface area of the composites increased with their BVO content, consistent with the findings of Yan et al. [7]. The BET surface areas followed the order BOS > BBA > BA(2) > BA(1) > BA(0.5) > AVO > BVO (Table 1). Generally, a larger surface area favors photocatalysis because it provides more adsorption and reactive sites.

PL spectra of the photocatalysts were obtained to examine their carrier separation efficiency during photocatalysis. A lower intensity of the PL peak of the photocatalyst corresponds to a lower probability of recombination of its photo-excited carriers and a greater charge transfer efficiency, which favors photocatalysis. PL spectra with an excitation wavelength of 400 nm were obtained at room temperature to study the separation efficiency of carriers (Fig. 4). The PL intensities followed the order BOS > BVO > BA (0.5) > AVO > BA(1) > BBA > BA(2). The PL intensities of BA(1), BA(2) and BBA were less than those of bare BOS, BVO and AVO, suggesting efficient charge transfer among BOS, BVO and AVO.

The valance and surface chemical compositions of BBA were determined using XPS, and the results are provided in Fig. 5. The Ag $3d_{5/2}$ and Ag $3d_{3/2}$ peaks at 367.2 and 373.2 eV in the high-resolution spectrum of Ag_{3d} (Fig. 5a) are characteristic of Ag^+ [21–23]. No Ag^0 is identified by peak fitting. The spectrum of Bi_{4f} (Fig. 5b) includes two characteristic peaks at 158.2 and 163.6 eV that arose from the Bi $4f_{7/2}$ and Bi $4f_{5/2}$ orbitals, respectively [14,24–26], and these are assigned to the +3 bismuth state, suggesting that the bismuth ions in BBA are in the trivalent state. Characteristic spin-orbit splitting of the V $2p_{3/2}$ and V $2p_{1/2}$ signals was observed at approximately 515.8 and 523.2 eV, respectively, corresponding to V^{5+} in BBA (Fig. 5c) [22,27,28]. Fig. 5d presents the asymmetrical O 1s signal and the peaks at 529.0, 529.4, 531.0 and 531.8 eV, which are associated with the Ag–O [29], Bi–O [29,30], V–O and –OH [14,31] bonds, respectively. The peaks at 530–531.4 eV are attributed to the lattice oxygen in the heterogeneous multi-phase photocatalysts [32]. Therefore, the peak at 531.0 eV was suggested to be associated with the V–O bond.

3.2. Evaluation of photocatalytic activity of synthesized photocatalysts

Fig. 6 presents the removal of RR2 by all synthesized photocatalysts. The efficiencies of removal of RR2 after 20 min of adsorption by BOS, BVO, AVO, BA(0.5), BA(1), BA(2) and BBA were 2%, 7%, 9%, 5%, 15%, 8% and 20%, respectively (Fig. 6a). RR2 cannot be effectively decolorized by adsorption. After 20 min of reaction, the percentages of RR2 that were removed by BOS, BVO, AVO, BA(0.5), BA(1), BA(2) and BBA with UV photocatalysis were 82%, 49%, 81%, 62%, 86%, 55% and 80%, respectively (Fig. 6b), and with Vis. photocatalysis were 52%, 26%, 17%, 6%, 53%, 18% and 77%, respectively (Fig. 6c). The photocatalysis of the decolorization of RR2 closely fitted the following pseudo-first-order equation [Eq. (1)] [3,15,16,22,32,33].

$$\ln\left(\frac{C_0}{C}\right) = kt \tag{1}$$

where C_0 and C represent the initial and residual concentrations of RR2 solution; t is the reaction time (h), and k is the reaction rate constant (h^{-1}).

A highly linear relationship was observed between $\ln(C_0/C)$ and irradiation time (Table 1). The k values of UV photocatalysis followed the order BA(1) > BOS > AVO > BB A > BA(2) > BA(0.5) > BVO and those of Vis. photocatalysis

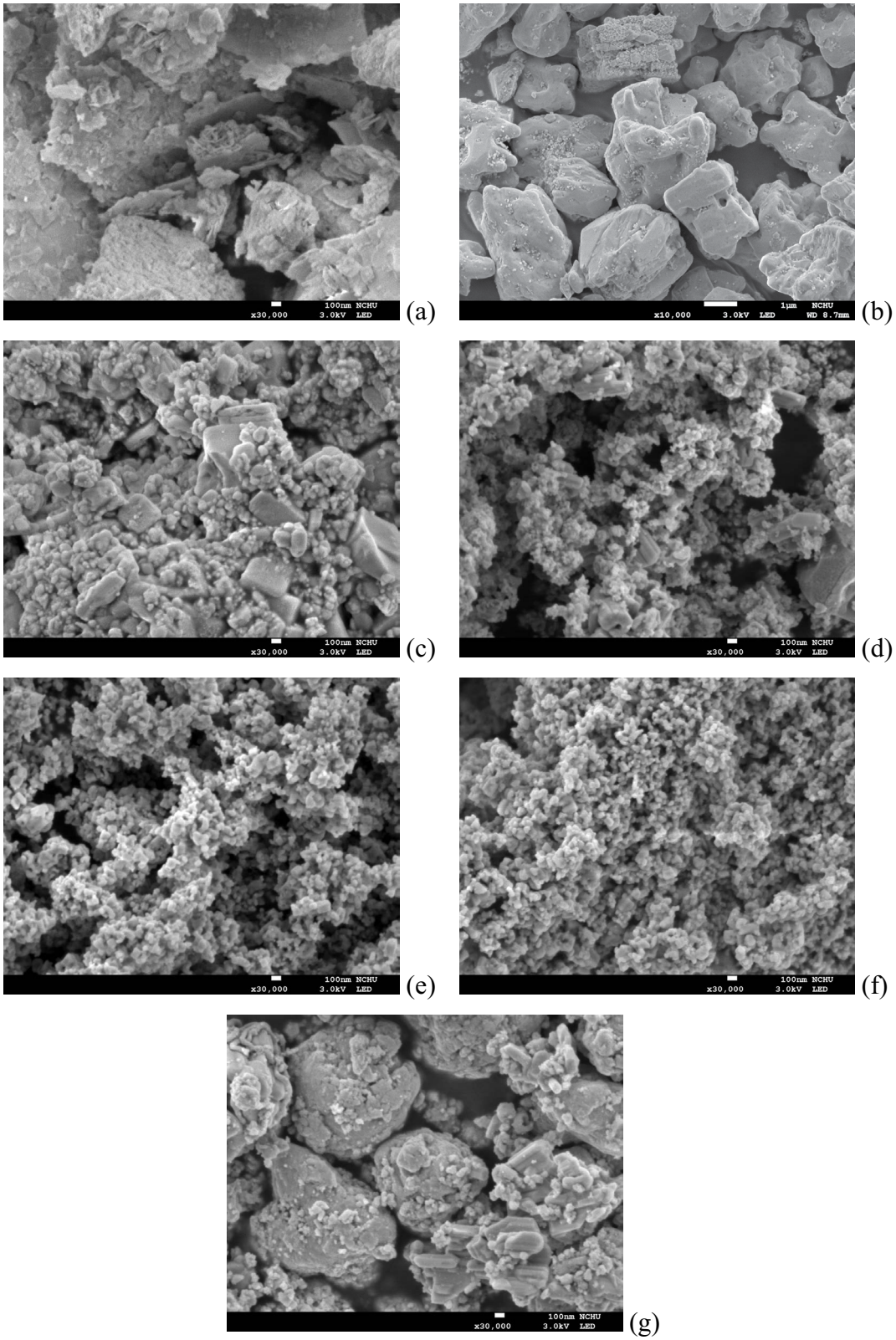

Fig. 2. SEM image of photocatalyst (a) BOS, (b) BVO, (c) AVO, (d) BA(0.5), (e) BA(1), (f) BA(2) and (g) BBA.

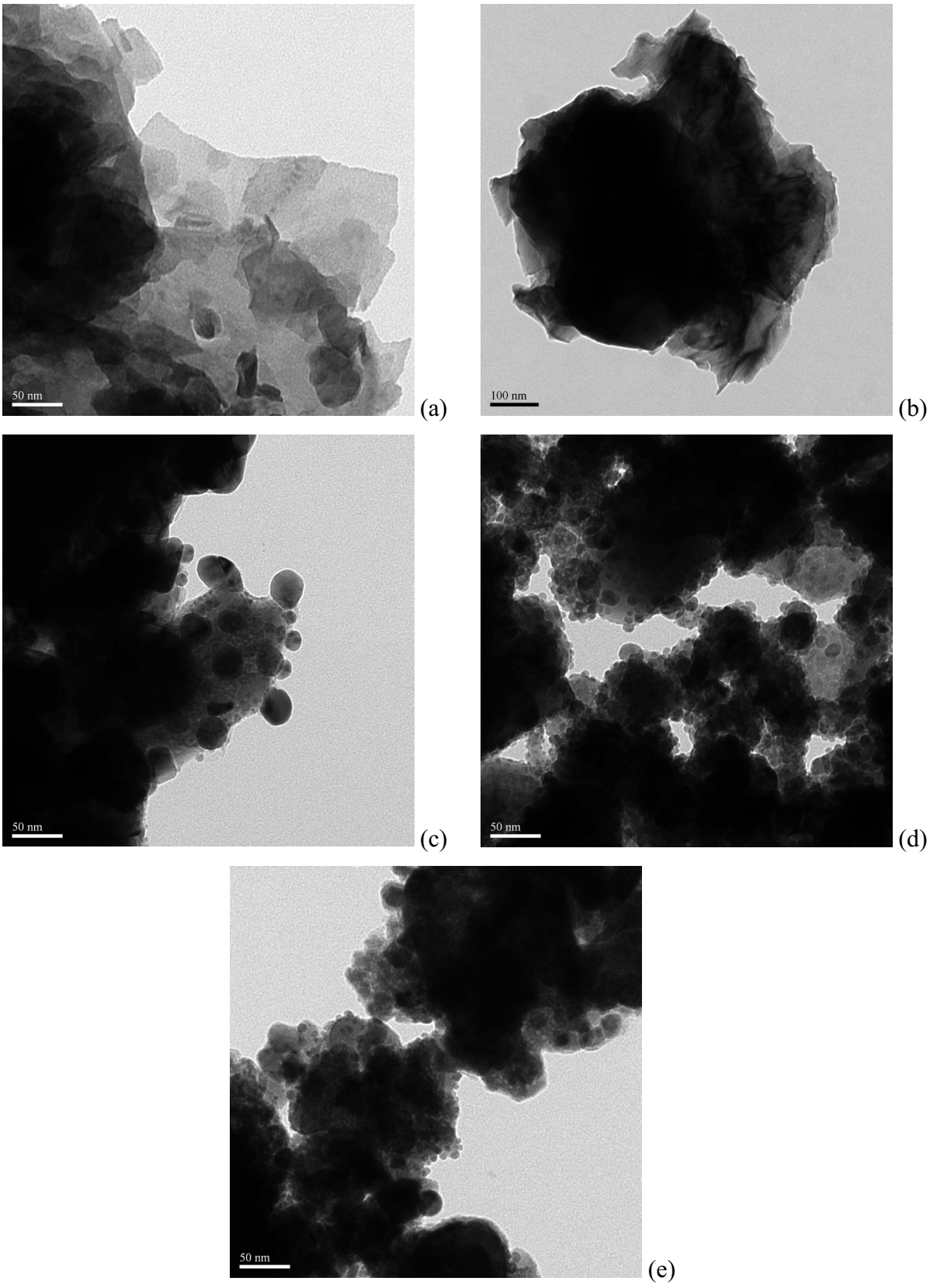

Fig. 3. TEM image of photocatalyst (a) BOS, (b) BVO, (c) AVO, (d) BA(1), and (e) BBA.

Table 1
Surface characteristics of synthesized photocatalysts

Photocatalysts	BET surface area	Bandgap	UV photocatalysis		Vis. photocatalysis	
	(m^2/g)	(eV)	k (h^{-1})	R^2	k (h^{-1})	R^2
BOS	18.6	3.0	4.55	0.999	1.87	0.997
BVO	0.08	2.4	2.02	0.974	0.29	0.776
AVO	2.18	1.8	4.23	0.967	0.21	0.928
BA(0.5)	2.77	1.9	2.15	0.967	0.08	0.820
BA(1)	4.21	2.3	5.77 (5.38)*	0.930 (0.990)*	1.69	0.980
BA(2)	4.55	2.3	2.71	0.983	0.54	0.992
BBA	11.34	1.8	3.50 (3.23)*	0.994 (0.985)*	2.59	0.993

()*: solar photocatalysis

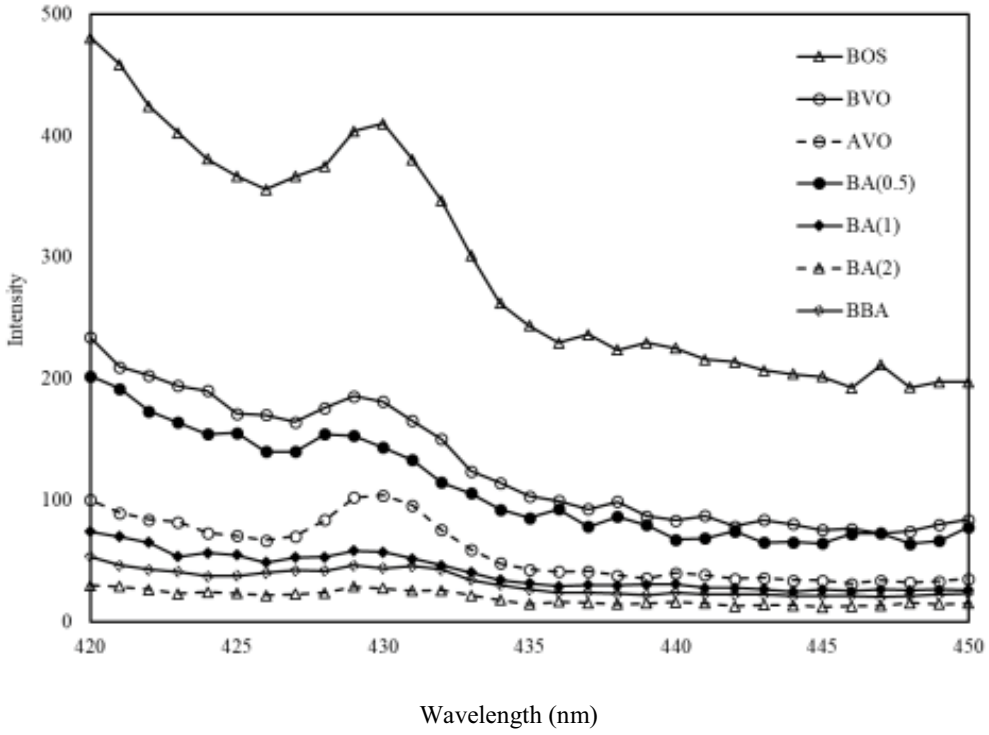

Fig. 4. PL spectra of synthesized photocatalysts.

followed the order BBA > BOS > BA(1) > BA(2) > BVO > AVO > BA(0.5) (Table 1). Under both UV and Vis. irradiation, a BVO/AVO molar ratio of unity was associated with the deposition of the amount of BVO nanoparticles on the AVO surface that maximized photocatalytic performance. Hu and Hu [34] and Chen et al. [35] suggested that when the amount of dopant exceeds its optimal value, it may provide recombination centers for the photo-generated electrons and h^+, reducing the thickness of the space-charge layer on the surface of each photocatalyst particle, and thereby reducing the absorption of photons. When the amount of BVO deposited is too low, the number of trapping sites for carriers increases with the amount of BVO deposited, and this effect has been proposed to prolong the lifetime of carriers, improving the photocatalytic activity. In contrast, if too much BVO is deposited, then the excess BVO may prevent the transfer of photo-generated electrons and thereby reduce the exposure of active sites owing to the extensive overlapping of BVO particles [9].

The k value of BBA in the Vis. photocatalysis of the removal of RR2 was almost 1.4, 8.9, 12.3 and 1.5 times those of BOS, BVO, AVO and BA(1), respectively. The outstanding Vis. photocatalytic performance of the BBA heterojunction was attributable to the synergistic properties of BOS and BA(1). Based on the PL study, the enhanced activity of BBA may be partially attributable to an increase in the efficiency of separation of photo-generated electron-hole pairs therein. The k values of BA(1) and BBA under solar irradiation were 5.38 and 3.23 h^{-1}, respectively (Table 1). Both BA(1) and BBA exhibited high photocatalytic activity

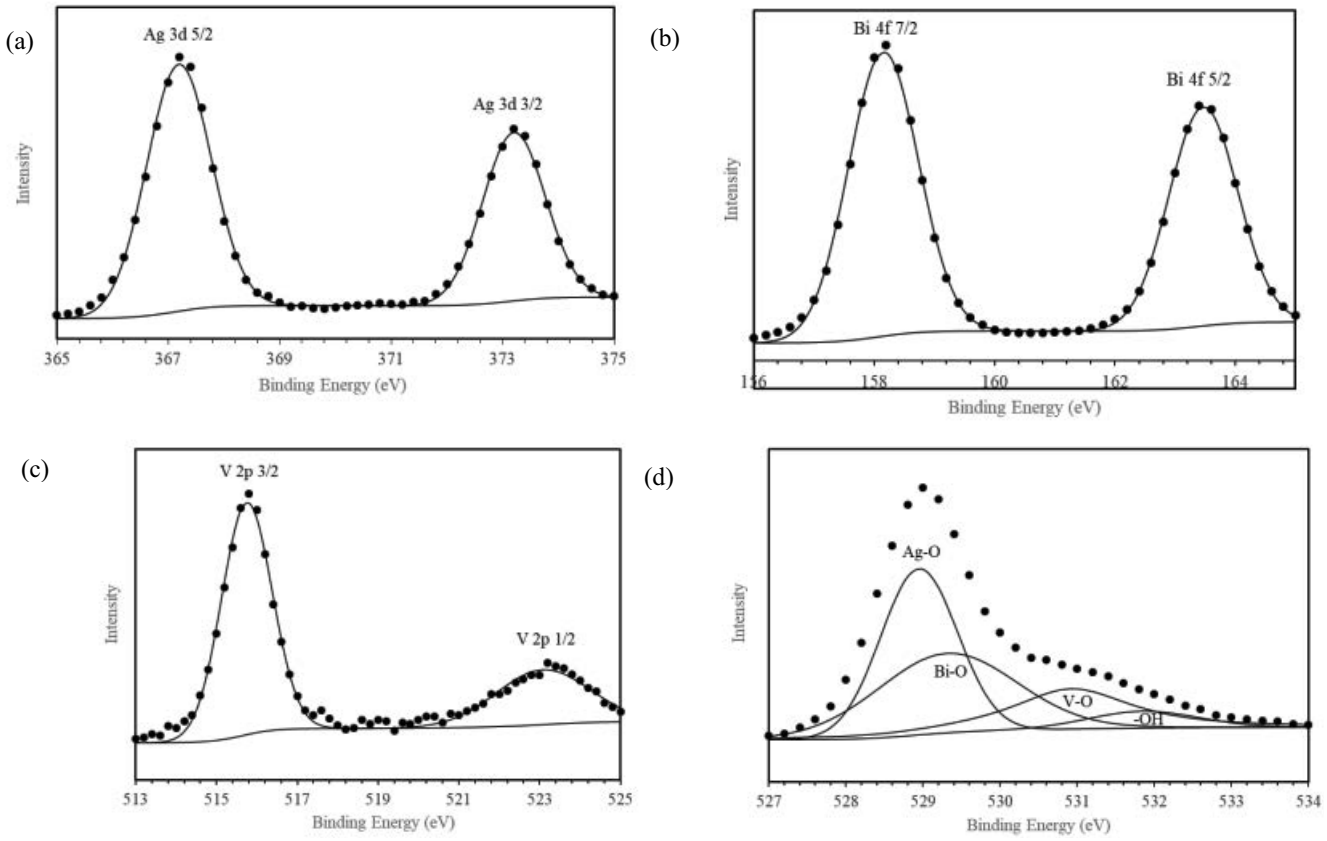

Fig. 5. XPS spectra of BBA (a) Ag_{3d}, (b) Bi_{4f}, (c) V_{2p}, and (d) O_{1s}.

under Vis. and solar irradiation. This study suggests that BA(1) was the best photocatalyst under UV and solar irradiation while BBA was the best photocatalyst under Vis. irradiation.

Radical trapping experiments were conducted to identify the main active species in the BBA heterojunction. Fig. 7 plots the photocatalytic degradation ratios of RR2 using various scavengers over the BBA heterojunction. Introducing IPA, EDTA-2Na or Cr(VI) into the BBA system changed the RR2 photodegradation percentages by 7%, 33% and 23%, respectively (Fig. 7). The addition of EDTA-2Na had a great inhibiting effect on the photocatalysis of the decolorization of RR2, relative to the use of no scavenger. The efficiency of degradation of RR2 was only slightly reduced by IPA, suggesting that •OH was not the primary active species. h^+ played the most important role in the photocatalytic degradation process in the BBA heterojunction, and $•O_2^-$ had a secondary effect.

After each run, the BBA was collected, washed using D.I. water to remove residual RR2, dried at 353 K, and then put into fresh RR2 solution to begin a new cycle. In the recycling experiments, all experimental conditions were exactly those in the first cycle. Fig. 8 displays the experimental results. The RR2 removal efficiency of BBA after one, two and three cycles under Vis irradiation was 95%, 87% and 78%, respectively (Fig. 8). The photocatalytic activity was lower in the third cycle perhaps due to the leaching of Ag from BBA or blocking by some by-products that had formed at the active sites of the BBA during photocatalysis. The stability of BBA should be improved in future work.

3.3. Mechanism of enhanced photocatalytic efficiency in BBA heterojunction

The efficient separation of photo-generated electron–hole pairs is well known to be important in photocatalysis. The valence band (VB) and conduction band (CB) edge potentials of each photocatalyst at the point of zero charge were calculated using Eqs. (2) and (3) [6,36–38]:

$$E_{CB} = X - E_e - 0.5E_g \quad (2)$$

$$E_{VB} = E_{CB} + E_g \quad (3)$$

where X is the absolute electronegativity of the semiconductors, given by the geometric mean of the absolute electronegativities of the constituent atoms. The absolute electronegativity is defined as the arithmetic mean of the atomic electron affinity and the first ionization energy. The X values for BOS, BVO and AVO are 5.95 [24], 6.04 [24] and 5.65 eV, respectively [33]. E_e represents the energy of free electrons on the hydrogen scale (4.5 eV) and E_{CB} and E_{VB} are the CB and VB edge potentials, respectively [38]. The E_{CB} values of BOS, BVO and AVO are determined to

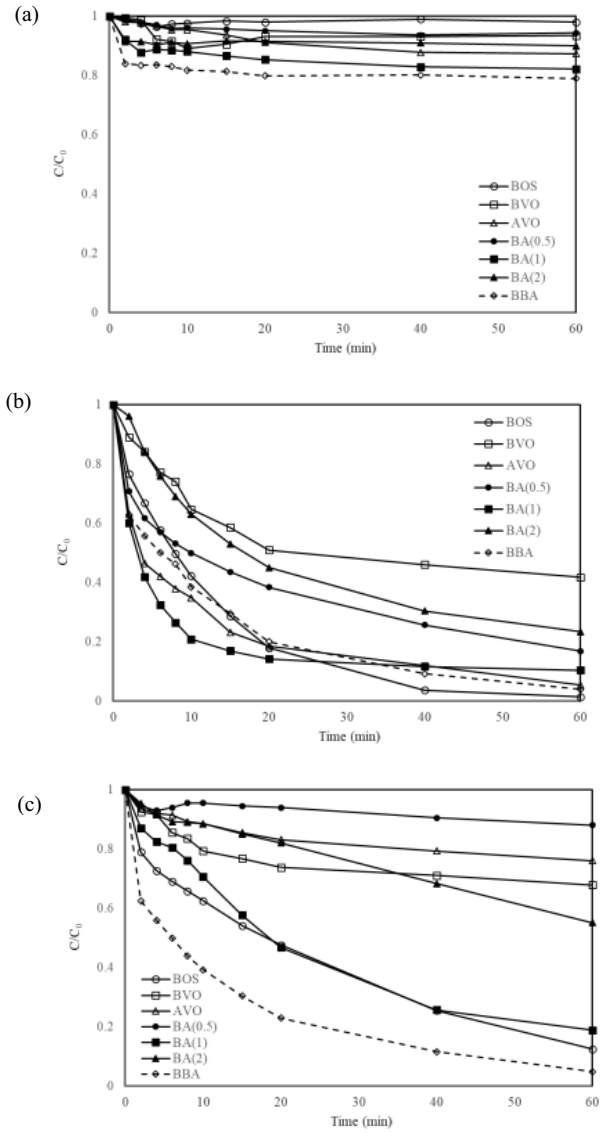

Fig. 6. Comparisons of removal of RR2 by all photocatalysts (a) adsorption, (b) UV photocatalysis, and (c) Vis. photocatalysis ([RR2] = 20 mg/L; pH = 3; [photocatalyst] = 0.5 g/L).

be –0.05, 0.34 and 0.25 eV, respectively, relative to the NHE level. The E_{VB} values of BOS, BVO and AVO are obtained as 2.95, 2.74 and 2.05 eV, respectively. These band edge positions of the photocatalysts were their potentials before contact. This difference between CB and VB potentials establishes a potential difference across the interface of the two photocatalysts, forming a heterojunction. Therefore, when they are in contact with each other, the band structures of BA(1) and BOS shells are reconfigured. The newly formed band structure has a lower potential of oxidation and a higher potential of reduction, greatly increasing both oxidative and reductive abilities [13]. Fig. 9 presents the energy band diagram and possible charge-separation process of BBA. In the BBA heterojunction, relatively useless e^- from the CB of BVO combined with h^+ from the VB of AVO. Furthermore, e^- (from the CB of AVO) combined with

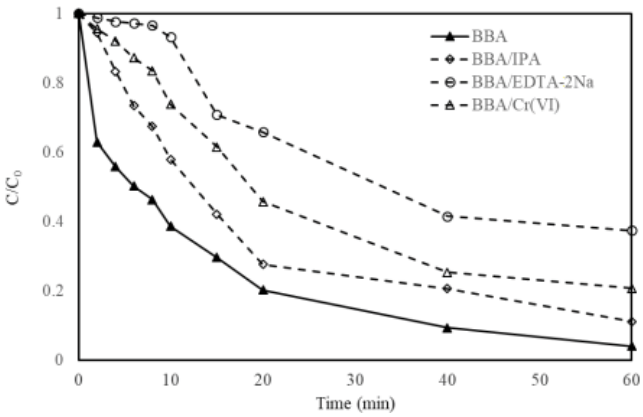

Fig. 7. Photocatalysis of RR2 in presence of scavengers for UV/BBA system ([RR2] = 20 mg/L; pH = 3; [BBA] = 0.5 g/L).

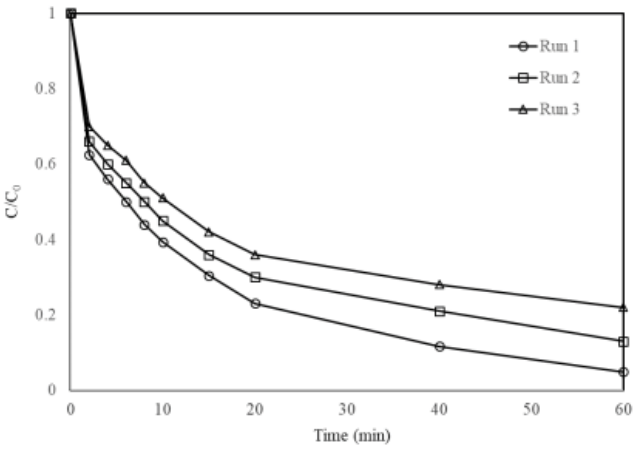

Fig. 8. Comparisons of cyclic photodegradation of RR2 in Vis/BBA system ([RR2] = 20 mg/L; pH = 3; [BBA] = 0.5 g/L).

h^+ (from VB of BOS) between AVO and BOS. Therefore, the useful e^- in the CB of BOS and the h^+ in the VB of BVO were all used. Hence, the recombination of the photo-generated electron-hole pairs was effectively inhibited; their lifetimes were prolonged, and thus the photocatalytic activity of the BBA heterojunction was greatly improved. The CB edge potential of BOS is more negative than that of $O_2/{}^{\bullet}O_2^-$ (–0.046 V/NHE) [39]; therefore, the photo-induced electrons may be trapped by the absorbed O_2, generating ${}^{\bullet}O_2^-$ [14]. The VB potential of BVO is more positive than the potential of ${}^{\bullet}OH/H_2O$ (2.38 V/NHE); accordingly, h^+ can trap H_2O and OH^- and oxidize them to form ${}^{\bullet}OH$. However, only a little of the absorbed H_2O and OH^- can be oxidized because most of the h^+ in the VB of BVO directly oxidizes RR2. BBA suppressed the recombination of photo-generated electron–hole pairs and improved the photocatalytic activities of BOS, BVO and AVO.

4. Conclusions

In this study, a novel BBA heterojunction was synthesized by a two-step hydrothermal/solvothermal process. Under both UV and Vis. irradiation, a BVO/AVO molar ratio

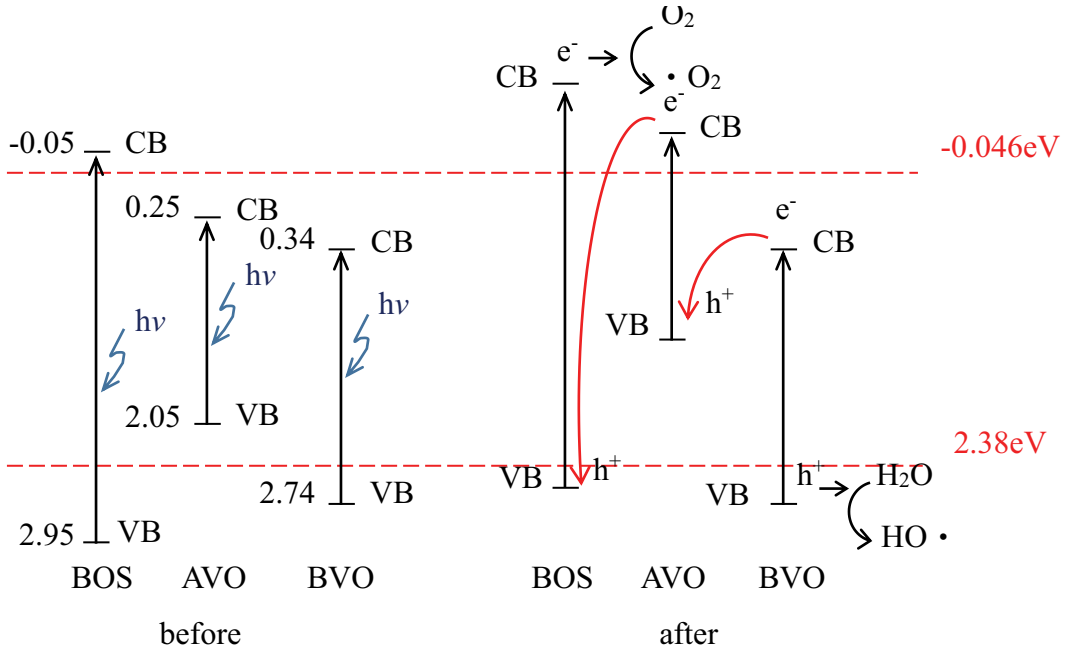

Fig. 9. Energy band diagram and possible charge-separation process of Vis/BBA system.

of unity optimized the amount of BVO that was deposited on the AVO surface, maximizing photocatalytic performance. The rate constants of Vis. photocatalysis followed the order BBA > BOS > BA(1) > BA(2) > BVO > AVO > BA (0.5). BA(1) was the best photocatalyst under UV and solar irradiation whereas BBA was the best photocatalyst under Vis. irradiation. This study suggests that in the BBA heterojunction, h^+ played the most important role in photocatalytic degradation. The enhancement by the use of BBA of the Vis. photocatalysis of the decolorization of RR2 is attributed to its heterojunction structure, which markedly increased the separation of the photo-generated electrons and h^+.

Acknowledgments

The authors would like to thank the Ministry of Science and Technology and National Kaohsiung University of Science and Technology, for financially supporting this research under Contract No. MOST 109-2221-E-992-050 and 109B01, respectively.

References

[1] R. Konta, H. Kato, H. Kobayashi, A. Kudo, Photophysical properties and photocatalytic activities under visible light irradiation of silver vanadates, Phys. Chem. Chem. Phys., 5 (2003) 3061–3065.
[2] A. Malathi, J. Madhavan, A. Muthupandian, P. Arunachalam, A review on $BiVO_4$ photocatalyst: activity enhancement methods for solar photocatalytic applications, Appl. Catal., A, 555 (2018) 47–74.
[3] C.H. Wu, C.Y. Kuo, C.D. Dong, C.W. Chen, Y.L. Lin, W.M. Chen, Synthesis of $Bi_2O_3/BiVO_4$ heterojunction with enhanced photocatalytic activity via single-step hydrothermal method, Desal. Water Treat., 172 (2019) 417–427.
[4] J. Zhang, M. Si, L. Jiang, X. Yuan, H. Yu, Z. Wu, Y. Li, J. Guo, Core-shell Ag@nitrogen-doped carbon quantum dots modified $BiVO_4$ nanosheets with enhanced photocatalytic performance under Vis-NIR light: synergism of molecular oxygen activation and surface plasmon resonance, Chem. Eng. J., 410 (2021) 128336, doi: 10.1016/j.cej.2020.128336.
[5] L. Liu, T. Hu, K. Dai, J. Zhang, C. Liang, A novel step-scheme $BiVO_4/Ag_3VO_4$ photocatalyst for enhanced photocatalytic degradation activity under visible light irradiation, Chin. J. Catal., 42 (2021) 46–55.
[6] L. Jiang, X. Yuan, G. Zeng, J. Liang, X. Chen, H. Yu, H. Wang, Z. Wu, J. Zhang, T. Xiong, In-situ synthesis of direct solid-state dual Z-scheme $WO_3/g\text{-}C_3N_4/Bi_2O_3$ photocatalyst for the degradation of refractory pollutant, Appl. Catal., B, 227 (2018) 376–385.
[7] M. Yan, Y. Wu, Y. Yan, X. Yan, F. Zhu, Y. Hua, W. Shi, Synthesis and characterization of novel $BiVO_4/Ag_3VO_4$ heterojunction with enhanced visible-light-driven photocatalytic degradation of dyes, ACS Sustainable Chem. Eng., 4 (2016) 757–766.
[8] R. Wang, L. Cao, Facile synthesis of a novel visible-light-driven $AgVO_3/BiVO_4$ heterojunction photocatalyst and mechanism insight, J. Alloys Compd., 722 (2017) 445–451.
[9] W. Zhao, Y. Feng, H. Huang, P. Zhou, J. Li, L. Zhang, B. Dai, J. Xu, F. Zhu, N. Sheng, D.Y.C. Leung, A novel Z-scheme $Ag_3VO_4/BiVO_4$ heterojunction photocatalyst: study on the excellent photocatalytic performance and photocatalytic mechanism, Appl. Catal., B, 245 (2019) 448–458.
[10] T. He, D. Wu, Y. Tan, Fabrication of $BiOI/BiVO_4$ heterojunction with efficient visible-light-induced photocatalytic activity, Mater. Lett., 165 (2016) 227–230.
[11] M. Mao, F. Chen, C. Zheng, J. Ning, Y. Zhong, Y. Hu, Facile synthesis of porous Bi_2O_3-$BiVO_4$ p-n heterojunction composite microrods with highly efficient photocatalytic degradation of phenol, J. Alloys Compd., 688 (2016) 1080–1087.
[12] P. Qiu, B. Park, J. Choi, M. Cui, J. Kim, J. Khim, $BiVO_4/Bi_2O_3$ heterojunction deposited on graphene for an enhanced visible-light photocatalytic activity, J. Alloys Compd., 706 (2017) 7–15.
[13] Y. Lee, M. Cui, J. Choi, J. Kim, Y. Son, J. Khim, Degradation of polychlorinated dibenzo-p-dioxins and dibenzofurans in real-field soil by an integrated visible-light photocatalysis and

solvent migration system with p-n heterojunction $BiVO_4/Bi_2O_3$, J. Hazard. Mater., 344 (2018) 1116–1125.
[14] J. Sun, X. Li, Q. Zhao, M.O. Tade, S. Liu, Construction of p-n heterojunction b-$Bi_2O_3/BiVO_4$ nanocomposite with improved photoinduced charge transfer property and enhanced activity in degradation of ortho-dichlorobenzene, Appl. Catal., B, 219 (2017) 259–268.
[15] C.H. Wu, C.D. Dong, C.W. Chen, Y.L. Lin, S.R. Jhu, Y.H. Lin, Enhanced visible light photocatalysis of $Bi_2O_3/BiVO_4$ and Bi_2O_3/Ag_3VO_4 heterojunction: effects of synthetic procedures, Desal. Water Treat., 209 (2021) 267–279.
[16] C.H. Wu, C.Y. Kuo, C.D. Dong, C.W. Chen, Y.L. Lin, Y.S. Kuan, Synthesis, characterization and photocatalytic activity of a novel Bi_2O_3/Ag_3VO_4 heterojunction photocatalyst, Desal. Water Treat., 198 (2020) 364–375.
[17] M. Su, C. He, V.K. Sharma, M.A. Asi, D. Xia, X.Z. Li, H. Deng, Y. Xiong, Mesoporous zinc ferrite: synthesis, characterization, and photocatalytic activity with H_2O_2/visible light, J. Hazard. Mater., 211–212 (2012) 95–103.
[18] Y. Chen, S. Yang, K. Wang, L. Lou, Role of primary active species and TiO_2 surface characteristic in UV-illuminated photodegradation of Acid Orange 7, J. Photochem. Photobiol., A, 172 (2005) 47–54.
[19] M.S. Gui, W.D. Zhang, Q.X. Su, C.H. Chen, Preparation and visible light photocatalytic activity of Bi_2O_3/Bi_2WO_6 heterojunction photocatalysts, J. Solid State Chem., 184 (2011) 1977–1982.
[20] H. Huang, K. Liu, K. Chen, Y. Zhang, Y. Zhang, S. Wang, Ce and F comodification on the crystal structure and enhanced photocatalytic activity of Bi_2WO_6 photocatalyst under visible light irradiation, J. Phys. Chem. C, 118 (2014) 14379–14387.
[21] J. Zhang, Z. Ma, Enhanced visible-light photocatalytic performance of Ag_3VO_4/Bi_2WO_6 heterojunctions in removing aqueous dyes and tetracycline hydrochloride, J. Taiwan Inst. Chem. Eng., 78 (2017) 212–218.
[22] J. Zhang, Z. Ma, $Ag_3VO_4/BiOIO_3$ heterojunction with enhanced visible-light-driven catalytic activity, J. Taiwan Inst. Chem. Eng., 88 (2018) 177–185.
[23] T.F. Chala, C.M. Wu, K.G. Motora, Rb_xWO_3/Ag_3VO_4 nanocomposites as efficient full-spectrum (UV, visible, and near-infrared) photocatalysis, J. Taiwan Inst. Chem. Eng., 102 (2019) 465–474.
[24] L. Chen, Q. Zhang, R. Huang, S. Yin, S. Luo, C.T. Au, Porous peanut-like Bi_2O_3-$BiVO_4$ composites with heterojunctions: one-step synthesis and their photocatalytic properties, Dalton Trans., 41 (2012) 9513–9518.
[25] Z. He, Y. Shi, C. Gao, L. Wen, J. Chen, S. Song, BiOCl/$BiVO_4$ p-n heterojunction with enhanced photocatalytic activity under visible-light irradiation, J. Phys. Chem. C, 118 (2014) 389–398.
[26] H. Li, Y. Sun, B. Cai, S. Gan, D. Han, L. Niu, T. Wu, Hierarchically Z-scheme photocatalyst of Ag@AgCl decorated on $BiVO_4$ (0 4 0) with enhancing photoelectrochemical and photocatalytic performance, Appl. Catal., B, 170–171 (2015) 206–214.
[27] X. Zou, Y. Dong, X. Zhang, Y. Cui, Synthesize and characterize of Ag_3VO_4/TiO_2 nanorods photocatalysts and its photocatalytic activity under visible light irradiation, Appl. Surf. Sci., 366 (2016) 173–180.
[28] Y. Xie, Y. Dai, X. Yuan, L. Jiang, L. Zhou, Z. Wu, J. Zhang, H. Wang, T. Xiong, Insight on the plasmonic Z-scheme mechanism underlying the highly efficient photocatalytic activity of silver molybdate/silver vanadate composite in Rhodamine B degradation, J. Colloid Interface Sci., 530 (2018) 493–504.
[29] S. Wang, Y. Guan, L. Wang, W. Zhao, H. He, J. Xiao, S. Yang, C. Sun, Fabrication of a novel bifunctional material of BiOI/Ag_3VO_4 with high adsorption-photocatalysis for efficient treatment of dye wastewater, Appl. Catal., B, 168–169 (2015) 448–457.
[30] X. Du, J. Wan, J. Jia, C. Pan, X. Hu, J. Fan, E. Liu, Photocatalystic degradation of RhB over highly visible-light-active Ag_3PO_4-Bi_2MoO_6 heterojunction using H_2O_2 electron capturer, Mater. Des., 119 (2017) 113–123.
[31] X. Ding, K. Zhao, L. Zhang, Enhanced photocatalytic removal of sodium pentachlorophenate with self-doped Bi_2WO_6 under visible light by generating more superoxide ions, Environ. Sci. Technol., 48 (2014) 5823–5831.
[32] L. Jing, Y. Xu, C. Qin, J. Liu, S. Huang, M. He, H. Xu, H. Li, Visible-light-driven $ZnFe_2O_4/Ag/Ag_3VO_4$ photocatalysts with enhanced photocatalytic activity under visible light irradiation, Mater. Res. Bull., 95 (2017) 607–615.
[33] S. Li, S. Hu, W. Jiang, Y. Liu, J. Liu, Z. Wang, Facile synthesis of flower-like Ag_3VO_4/Bi_2WO_6 heterojunction with enhanced visible-light photocatalytic activity, J. Colloid Interface Sci., 501 (2017) 156–163.
[34] X. Hu, C. Hu, Preparation and visible-light photocatalytic activity of Ag_3VO_4 powders, J. Solid State Chem., 180 (2007) 725–732.
[35] S. Chen, W. Zhao, W. Liu, H. Zhang, X. Yu, Y. Chen, Preparation, characterization and activity evaluation of p-n junction photocatalyst p-$CaFe_2O_4$/n-Ag_3VO_4 under visible light irradiation, J. Hazard. Mater., 172 (2009) 1415–1423.
[36] S. Wang, D. Li, C. Sun, S. Yang, Y. Guan, H. He, Synthesis and characterization of g-C_3N_4/Ag_3VO_4 composites with significantly enhanced visible-light photocatalytic activity for triphenylmethane dye degradation, Appl. Catal., B, 144 (2014) 885–892.
[37] X. Meng, Z. Zhang, Bismuth-based photocatalytic semiconductors: introduction, challenges and possible approaches, J. Mol. Catal. A, 423 (2016) 533–549.
[38] Q. Shi, W. Zhao, L. Xie, J. Chen, M. Zhang, Y. Li, Enhanced visible-light driven photocatalytic mineralization of indoor toluene via a $BiVO_4$/reduced graphene oxide/Bi_2O_3 all-solid-state Z-scheme system, J. Alloys Compd., 662 (2016) 108–117.
[39] N. Tian, H. Huang, Y. He, Y. Guo, T. Zhang, Y. Zhang, Mediator-free direct Z-scheme photocatalytic system: $BiVO_4$/g-C_3N_4 organic-inorganic hybrid photocatalyst with highly efficient visible-light-induced photocatalytic activity, Dalton Trans., 44 (2015) 4297–4307.